MOLECULAR IMAGING AND BIOLOGY

Mol Imaging Biol (2019) 21:436–446
DOI: 10.1007/s11307-019-01324-7

Published Online: 25 February 2019

WMIS World Molecular Imaging Society

Check for updates

RESEARCH ARTICLE

Quantitative Imaging of Morphometric and Metabolic Signatures Reveals Heterogeneity in Drug Response of Three-Dimensional Mammary Tumor Spheroids

V. Krishnan Ramanujan [1,2,3,4]

[1]*Metabolic Photonics Laboratory, Departments of Surgery and Biomedical Sciences, Cedars-Sinai Medical Center, 8700 Beverly Blvd. Davis 6067, Los Angeles, CA, 90048, USA*
[2]*Department of Biomedical Sciences, Cedars-Sinai Medical Center, 8700 Beverly Blvd., Los Angeles, CA, 90048, USA*
[3]*Biomedical Imaging Research Institute, Cedars-Sinai Medical Center, 8700 Beverly Blvd., Los Angeles, CA, 90048, USA*
[4]*Samuel Oschin Comprehensive Cancer Institute, Cedars-Sinai Medical Center, 8700 Beverly Blvd., Los Angeles, CA, 90048, USA*

Abstract

Purpose: In order to monitor the drug responses of three-dimensional mammary tumor spheroids and to elucidate the role of inter- and intra-spheroid heterogeneity in determining drug sensitivity in the spheroids, an integrated image analysis framework was developed for morphometric and metabolic characterization of the three-dimensional tumor spheroids.

Procedure: Three-dimensional spheroid cultures of primary mammary tumor epithelial cells isolated from freshly excised tumors from a transgenic mouse model of adenocarcinoma (MMTV-PyMT) were imaged by using vital dyes and mitochondrial membrane potential markers. Custom-developed java and python program codes facilitated image processing, numerical computation, and graphical analysis of large datasets generated from the experiments. A panel of cancer drugs (rapamycin, BEZ235, MK2206, and flavopiridol) was tested to determine the degree of drug sensitivity as well as heterogeneity in drug response.

Results: A new quantitative metric (growth/toxicity) was developed based on morphometric parameters that were found to track the growth and apoptotic cell populations. Further, this study identified two parameters, namely, skew and kurtosis—which report the spatial heterogeneity in mitochondrial metabolism within the spheroids. The results of this study show that three-dimensional tumor spheroids selectively respond to cancer drugs depending on the specific metabolic pathways (AKT inhibition pathway in the present study), and there exists significant heterogeneity in the untreated tumor spheroids. Drug sensitivity of the spheroids was found to be associated with significant alterations in mitochondrial heterogeneity within the spheroids.

Conclusions: In conclusion, the quantitative imaging of morphometric and metabolic analysis in large image datasets can serve as an excellent tool box for characterizing tumor heterogeneity in three-dimensional tumor spheroids and potentially, in intact tumors as well.

Key words: Breast cancer, Three-dimensional spheroids, Mammary tumor organoids, Drug response, Mitochondria, Tumor heterogeneity, Image analysis

Electronic supplementary material The online version of this article (https://doi.org/10.1007/s11307-019-01324-7) contains supplementary material, which is available to authorized users.

Correspondence to: V. Ramanujan; *e-mail:* Ramanujanv@csmc.edu

Introduction

Breast cancer is one of the leading causes of cancer-related mortality and morbidity in women worldwide [1, 2]. In the past few decades, tremendous improvements have contributed effectively to improving the diagnostic accuracy as well as increasing survival rates in women diagnosed with breast cancer. However, the true value of these advancements is also mitigated by the different ways by which cancer cells evolve their survival strategies and develop their resistance to therapeutic interventions [3]. Adding to this complexity is the realization that human breast neoplasms are highly heterogeneous, thereby introducing significant variability in patient response to treatments [4–9]. Even though clinical diagnosis and other high-resolution imaging methods offer an excellent framework for tumor detection *in vivo*, these methods fail miserably in detecting tumor heterogeneity at the single-cell level. In the context of single-cell analysis, multiple pathology workflows have been valuable in addressing this knowledge gap [10]. However, these pathology analyses are often carried out in 4–8-µm-thick tumor slides and are therefore not amenable to mechanistic understanding of living tumor cell growth patterns in three-dimensional (3D) architectures. In recent times, tumor organoid models are being evaluated for their utility in providing the much-needed flexibility for analyzing growth characteristics and drug response characteristics of tumor cells in native 3D physiological environments [11]. For example, from the earliest 3D scaffolds of matrigel to the current organ-on-a-chip model, the field is continually improving. This ability to culture and analyze tumor cells in 3D environment has given the researchers an unprecedented advantage to ask mechanistic questions while increasing the modular complexity of the 3D scaffold. In particular, 3D cell culture models have given a conceptual framework for testing and triaging multiple drug candidates in 3D primary tumor cell cultures before testing in human patients [12]. However, in order to translate the discoveries from 3D tumor cell culture models to actionable clinical practice, it is not only sufficient to obtain good quality dataset but also necessary to have a thorough quantitative understanding of the 3D dataset. It is not sufficient to know which drug works better but it is equally important to know how much of this drug is actually accessed by tumor cells in a 3D growth architecture and what is the variability in tumor cell response in a 3D environment, *etc*., In addition to these quantitative analysis steps, it will be critical to assess how these metrics vary within 3D growth structures and between the different 3D growth structures—thereby offering insights on the intra- and inter-tumor heterogeneity in real-life settings. The present study aims to address three questions: (a) what are the critical quantitative metrics that best describe morphometric and metabolic characteristics of tumor cells in 3D growth patterns? (b) How do these metrics alter while tumor cells in 3D growth patterns respond to drug treatments? (c) How does this quantitative analysis offer a viable approach to analyzing tumor cell heterogeneity in 3D tumor growth model? This study seeks to find answers to these questions using a preclinical mouse model of breast adenocarcinoma (mimicking human luminal breast cancers) and a fluorescence-imaging approach for characterizing the 3D mammary organoids generated from the primary tumor cells obtained from the aforementioned mouse model. This author developed an integrated image-analysis framework by using java scripts and python programs, to facilitate image processing, numerical computation, and graphical plotting.

Materials and Methods

Cell Culture

A transgenic mouse (MMTV-PyMT) model of mammary adenocarcinoma was used in this study. Primary mammary tumors appear spontaneously in this mouse at the age of 6 weeks and continue through 16 weeks when they usually metastasize to the lungs [13]. The primary mammary tumor epithelial cells used in this study were isolated from freshly excised tumors (~12–16 weeks) [14]. For culturing the cells in three-dimensional (3D) architecture, we optimized a reproducible method of adding 10 % matrigel in mammocult medium (StemCell Technologies, Cambridge, MA, USA). For the drug response studies, cells were plated in 3D architectures as described above and drugs were added 16 h after plating. The drug treatment responses were monitored at 24 h, 48 h, and 72 h after the addition of drugs.

Imaging

Live 3D spheroid cultures were imaged either on a wide-field microscope (Olympus IX70) and/or on a confocal microscope (Leica SP5). Two-photon fluorescence imaging was adopted to measure mitochondrial metabolic signals in 3D spheroids as described earlier [14]. The fluorogenic probes used in this study, calcein-AM (catalog #C3100MP), mitotracker green (catalog #M7514), and tetramethyl rhodamine methyl ester (TMRM) (catalog #T668) were purchased from (Thermo Fisher Scientific Corporation, Waltham, MA, USA). Calcein-AM labeling was used to achieve high-contrast images of the viable spheroids. Mitotracker green label selectively stains live mitochondria and hence is a good indicator of mitochondrial mass while TMRM is more a functional probe that accumulates within the mitochondrial depending on the relative mitochondrial membrane potential [15]. Together, TMRM and mitotracker green imaging can give reliable differences between the mitochondrial metabolic status of the individual 3D mammary tumor spheroids [14]. For all the data presented here, the live 3D spheroids were labeled with either 100 nM Calcein-AM or 200 nM each of the mitochondrial probes (TMRM/mitotracker green)

for 30 min at 37 °C and washed with phosphate-buffered saline before imaging at room temperature.

Image Analysis

Images acquired from the two imaging configurations were analyzed by custom-made image analysis modules. First, the images were pre-processed using the ImageJ software and multiple size/shape (*i.e.*, morphometric) parameters were measured using custom-made macros written in java script. This step ensured that all the images were treated in identical way eliminating potential artifacts arising from human bias. Along with the morphometry parameters, higher moments of intensity were also measured, namely, skew and kurtosis, using the built-in ImageJ modules. Skew and kurtosis parameters inform how a given distribution deviates from a Gaussian (normal) distribution [16]. Skew parameter gives information on the symmetry of the distribution while kurtosis refers to the "pointedness" or "flatness" of the distribution. Secondly, a series of custom-made programs written in python language were created and the ImageJ-analyzed measurement data were fed as inputs to the python programs. This step included merging of multiple datasets into a single file for statistical analysis, analyzing *xyz* stacks to plot *z* axis profiles of various parameters of interest as well as calculating pair-correlation functions as described later in the text. Final graphs presented in this manuscript were either plotted by using the custom-made python programs and/or by using Origin 8.0 graphical software (OriginLab, Northampton, MA, USA). Specific image analysis details are given in the "Results" section.

Statistics

Data presented are mean ± SE from at least three independent experiments unless otherwise mentioned. Statistical significance was estimated based on Student's *t* test ($p < 0.05$).

Results

Optimization of 3D Spheroid Culture and Image Analysis Framework

Figure 1a shows a schematic of the mouse mammary gland with the ductal morphology and the surrounding fat pad. Also shown are the representative histology images obtained from thin slices of a normal mammary gland tissue and a mammary adenocarcinoma tissue. Earlier studies have reported the use of various scaffolds and culture medium for generating 3D spheroids. The generation and culture of 3D mammary tumor spheroids was optimized in the author's laboratory, and these spheroids mimic the early tumor acini (solid arrows in Fig. 1c) in the tumor *in vivo*. This was achieved by combining 10 % matrigel in the mammocult as shown in Fig. 1d, e. The 3D spheroids showed a dramatic increase in mRNA level of milk fat globule-EGF protein 8 (Mfge8, a luminal marker) as compared to the 2D monolayer cultures indicating that 3D culture mimics the *in vivo* mammary gland condition well. (Suppl Fig. S1, see Electronic Supplementary Material (ESM)). Next, it was tested to confirm if there are measurable changes in the 3D spheroid shape and size with duration. Figure 1f, g summarizes these findings with a representative size metric, the Feret diameter as measured by the image analysis protocol. Traditionally, mean fluorescence is a key parameter that is monitored in any imaging dataset. In addition to the mean fluorescence, in the present study other parameters were also measured, namely, two size parameters (area and Feret diameter), three shape parameters (circularity, aspect ratio, solidity), and two higher-order moments of the mean fluorescence (skew and kurtosis). The inter-relationship between these various parameters is shown in the pair-correlation matrix (Fig. 1h) as well as in supplemental data (Fig. S2).

Quantitative Metric for Monitoring Growth and Toxicity in 3D Spheroids

Various assays have been reported for monitoring cellular viability and drug response characteristics in monolayer cultures. However, there is paucity of strategies for reliably monitoring growth characteristics in cells growing in 3D cultures. In this paper a novel approach is presented to rapidly assess growth and toxicity of mammary tumor cells in 3D spheroids. To demonstrate this approach, the mammary tumor epithelial cells were cultured in 3D architectures as described above and were exposed to a known apoptosis inducer, 1 μg/ml staurosporine. Analysis of frequency histograms of Feret diameter indicated a bimodal distribution pertaining to two different size spheroids with mean Feret diameter, 13 μm and 63 μm, respectively. With an increase in culture duration (24 to 72 h), this second population (larger spheroids) was observed to grow in size leading to a larger area under curve (AUC) in the case of the untreated mammary spheroids. On the other hand, the staurosporine-treated spheroids clearly showed the opposite trend indicating that toxicity-induced disintegration of larger spheroids outweighs the growth potential of them. We define a {growth/toxicity} parameter as a ratio of AUC of second population (larger spheroids) to that of the first population (smaller spheroids). As shown in Fig. 2c, this quantitative metric can serve as a surrogate measure of cell viability in 3D cultures.

Mitochondrial Metabolism as a Sensitive Heterogeneity Metric in 3D Spheroids

A salient difference between 3D spheroid culture and 2D monolayer culture is the emergence of hypoxic regions

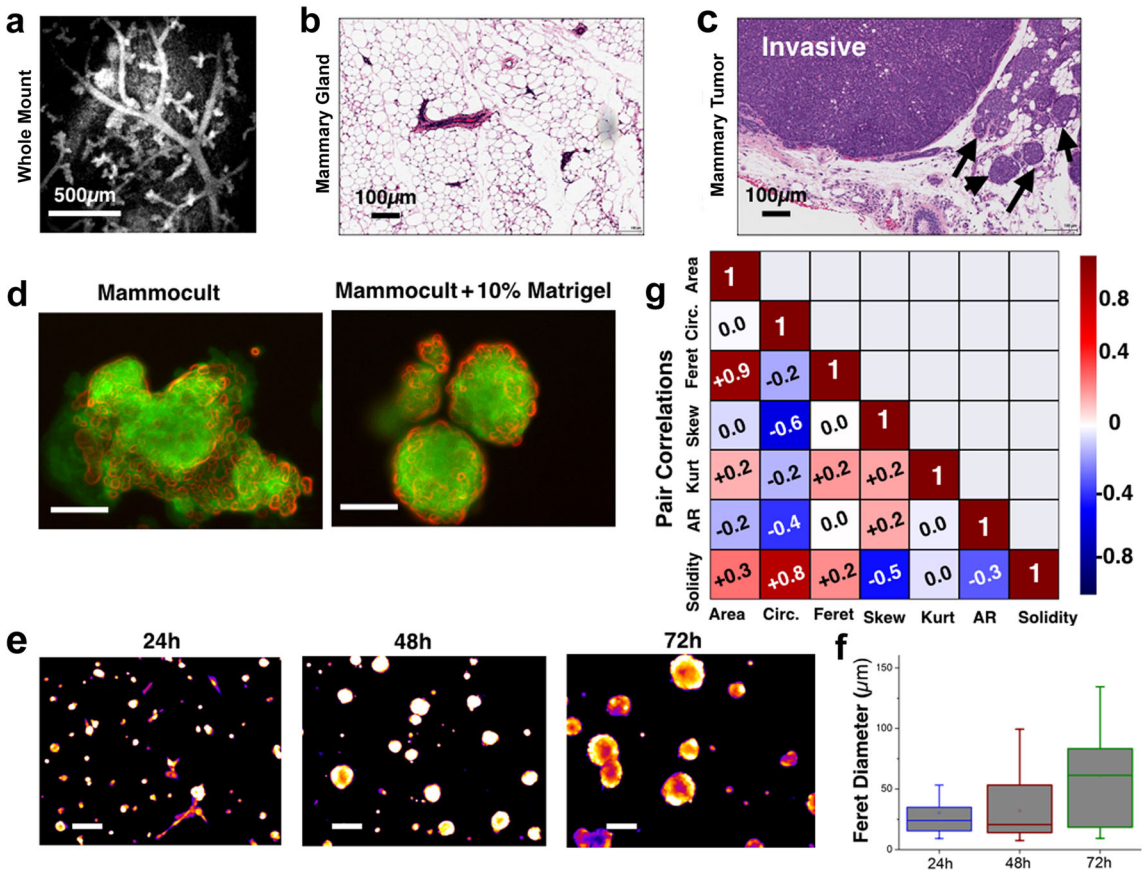

Fig. 1 Setting up an integrated platform for generating and characterizing 3D tumor spheroids. **a** Three-dimensional reconstructed image of a whole mount of normal murine mammary gland section labeled with carmine dye. **b**, **c** Histology images of normal mouse mammary gland section and mouse adenocarcinoma obtained from a female PyMT mouse (12 weeks). **d** Primary tumor epithelial cells isolated from mouse tumors. Primary three-dimensional spheroids were cultured in in mammocult medium with or without 10 % matrigel added to the medium. Addition of Matrigel increased the density and compactness of the cells within the spheroids—mimicking the tumor acini within the mouse tumor tissue shown by arrows in **c**. **e** Representative 3D spheroids shown after 24-h, 48-h, and 72-h cultures. **f** Feret diameter estimates show that there is a clear increase in spheroid volume with time. **g** In addition to Feret diameter, other size and shape parameters were also measured from the images. Pair correlations between two size parameters (area, Feret diameter), two intensity moments (skew, kurtosis), and two shape parameters (circularity, aspect ratio, solidity) are shown.

in the 3D cultures. Hypoxia has been earlier shown to modulate the balance between glycolytic and mitochondrial metabolism, thereby impacting cancer cell growth *in vivo*. Furthermore, the response of the cancer cells to drugs may also depend on the nature of metabolic (*e.g.*, mitochondrial, glycolytic, or hypoxic) signals prevalent in the cancer cell microenvironment. Thus, it will be valuable to assess the differential mitochondrial function status within the 3D spheroids. Towards this direction, the 3D spheroids were labeled with mitotracker green (the vital mitochondrial dye) and TMRM (a mitochondrial-potential-dependent dye) as shown in Fig. 3a. Two-photon fluorescence imaging was carried out to acquire *xyz* stacks from individual spheroids ($\Delta z =$ 1 μm) and image analysis was performed as described above. Since mitochondrial function critically depends on the availability of oxygen, there is a significant drop in the mitochondrial membrane potential (as measured through TMRM fluorescence) even though there are viable mitochondria present in the core of the spheroid (as measured through mitotracker green fluorescence). Figure 3b shows the mean fluorescence and its higher-order moments, namely, standard deviation, skew, and kurtosis, as explained in the "Materials and Methods" section earlier. As can be seen from these plots, the skew and kurtosis parameters are quite different with respect to TMRM fluorescence as compared with those of mitotracker green fluorescence. This differential *z*-profile points out to an interesting possibility that the skew and kurtosis parameters can serve as sensitive measures of spatial heterogeneity within the spheroids. In the present case, these two parameters reveal a strong spatial heterogeneity in mitochondrial metabolism in live 3D spheroids along the *z* axis.

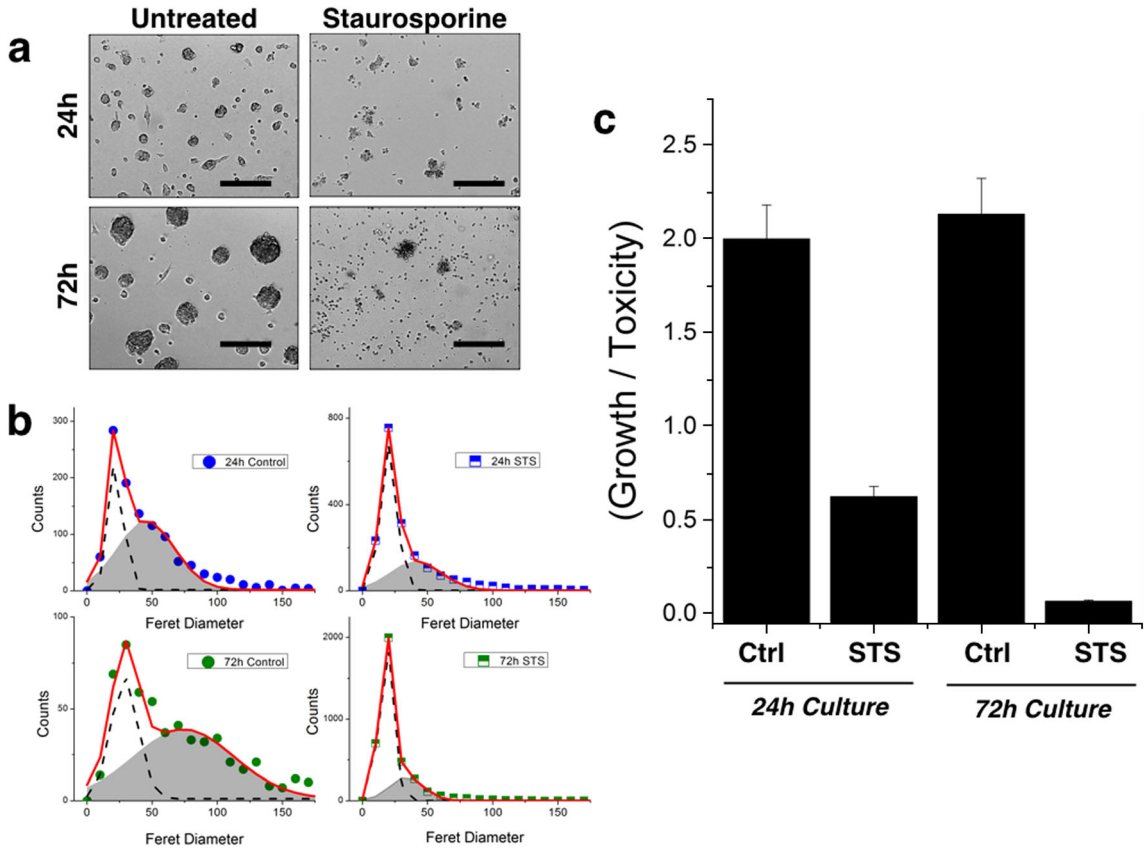

Fig. 2 Morphometry-based definition of growth and toxicity in 3D tumor spheroids. **a** Bright-field images acquired at 24-h and 72-h cultures of untreated and (1 μg/ml) staurosporine-treated of mammary 3D spheroids. Scale bars = 20 μm. **b** Size and shape parameters were measured as demonstrated in Fig. 1. Representative frequency histogram plots of Feret diameter as determined from 24-h and 72-h cultures. A two-population model Gaussian fit to each of these histograms delineated two populations of 3D spheroids with mean Feret diameters 13 μm and 63 μm for the populations 1 and 2, respectively. Untreated mammary spheroids clearly show an increase in both the number and the size of larger spheroids with time while the staurosporine-treated spheroids display a pronounced decrease in the size and the number of the larger spheroids with a concomitant increase in the number of smaller spheroids and individual cells. **c** Area under the curves (AUC) from these two-population model curves were computed and we define here a {growth/toxicity} parameter calculated as {AUC(peak2)/AUC(peak1)} ratio. As can be seen, this ratio parameter reveals a situation where the untreated spheroids balance nutrient-derived spheroid growth with the inherent attrition and/or toxicity. This balance is severely affected in spheroids treated with an apoptosis inducer, staurosporine.

Quantitative Estimation of Differential Drug Sensitivity of the 3D Tumor Spheroids

In order to determine the robustness of the present image analysis approach in detecting subtle changes during cancer cell response to drugs, a panel of cancer drugs was tested for their efficacy in eliciting cell death in PyMT 3D mammary tumor spheroids. This panel included a mTOR inhibitor (500 nM rapamycin), dual mTOR1/mTOR2 inhibitor (10 μM BEZ235), a selective AKT inhibitor (1 μM or 10 μM MK2206), and a potent inhibitor of cyclin-dependent kinases (100 nM or 1 μM flavopiridol) [17–23]. The rationale for this choice of drugs stems from our earlier observations and other studies where the hyperactivation of PI3K/AKT pathway is known to regulate the tumorigenic pathway in this PyMT adenocarcinoma model. The primary mammary spheroids were cultured as described above, and 16 h after plating the cells, drug treatment as shown was initiated in the 3D culture medium. Calcein-AM-labeled spheroids were imaged and analyzed as described above. Figure 4 shows a representative set of images for the various drug treatment conditions. {Growth/toxicity} ratio was estimated for three independent trials, and Fig. 4b summarizes the mean ± SE of this metric. The AKT-inhibitor MK2206 and the CDK-dependent kinase inhibitor flavopiridol showed the most significant differences in drug sensitivity. Since the Feret diameters for the two populations of spheroids were nearly similar (Fig. 4c), it can be surmised

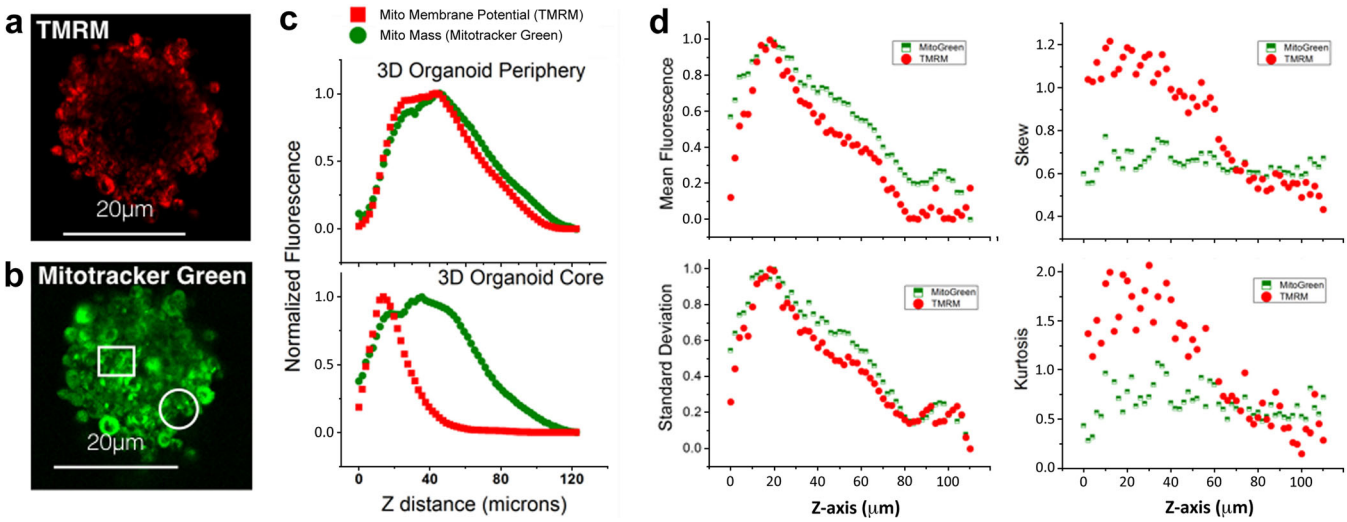

Fig. 3 Mitochondrial metabolic characterization of intra-spheroid heterogeneity. Two-photon fluorescence images of 3D spheroid labeled with **a** the mitochondrial membrane potential marker tetramethyl rhodamine methyl ester (TMRM) and **b** the mitochondrial vital stain mitotracker green. Three-dimensional *xyz* stacks were collected in live 3D spheroids with 810-nm two-photon excitation. The core of the spheroid shows a significantly reduced TMRM staining as compared to that in the periphery of the spheroid. On the other hand, mitotracker green signal was observed to be uniform at the core and at the periphery. **c** The variation of the normalized fluorescence signals at representative regions of interest (square indicated in the core and circle indicated in the periphery) along the *z* axis. **d** A more detailed morphometric analysis of *z* axis profiles included computing mean values of multiple size/shape parameters in each *z* plane ($n = 58$ planes with $\Delta z = 2$ μm). Representative *z* axis variation of mean fluorescence and its higher-order moments, namely, standard deviation, skew, and kurtosis, are shown. Interestingly, the higher-order moments, skew, and kurtosis could clearly show the differential metabolism as probed by TMRM and mitotracker green staining.

that the observed drug sensitivity stems mainly from the decrease in the number of larger spheroids upon treatment with MK2206 and flavopiridol. A comparison with the traditional MTT-based measurements of cell viability with the results obtained using the current image analysis method showed an excellent agreement, thereby validating the present method (Supplemental Fig. S3, ESM). It is also possible that disintegration of the 3D spheroids during apoptosis can lead to the shift in balance from larger to smaller spheroids as shown Fig. 4d, where representative line profiles are compared for three cases. The full width at half maximum (FWHM) of individual peaks in these profiles corresponds to the linear dimensions of the spheroids. Further, the concentration-dependent effects on the drug sensitivity revealed that the sub-optimal dosages of flavopiridol (100 nM) can induce larger variance and hence poor drug sensitivity in 3D spheroids (Fig. 4e).

Combination of Morphometric and Metabolic Analyses Can Give Robust Information on the Heterogeneity in Drug Response Within the 3D Spheroids

In order to determine if the observed drug sensitivity with MK2206 and flavopiridol is uniform between the spheroids (inter-spheroid heterogeneity) and within individual spheroids (intra-spheroid heterogeneity), the live spheroids were labeled with mitochondrial membrane potential marker, TMRM. Confocal image stacks (*xyz*) of individual spheroids (~20–30 spheroids per condition) for untreated and drug-treated conditions (Fig. 5a). A custom-developed image analysis protocol processed multiple spheroid datasets were acquired and the morphometric size and shape parameters as well as intensity parameters were computed for each *xy* plane. By comparing the *z* axis profile of various parameters in individual spheroids, the statistical spread of mean TMRM fluorescence as well as skew and kurtosis parameters could be determined. Volume measurements in 3D spheroids as probed by TMRM fluorescence correspond to functional mitochondrial maps in each spheroid, thereby providing a robust measure of metabolic heterogeneity in untreated and drug-treated conditions. Figure 5b reveals that the TMRM-based spheroid volumes were significantly lower in MK2206-treated spheroids but not in those treated with 100 nM flavopiridol. This is in good agreement with the morphometry-based analysis (Fig. 4e). As developed in Fig. 3, *z*-profile of skew and kurtosis can offer valuable insights into the intra-spheroid heterogeneity (*i.e.*, internal variation in mitochondrial metabolism within the spheroids). Significant difference was also found in skew and kurtosis parameters upon treatment with MK2206 pointing out to an interesting possibility that reduction in intra-tumor-spheroid heterogeneity may be a

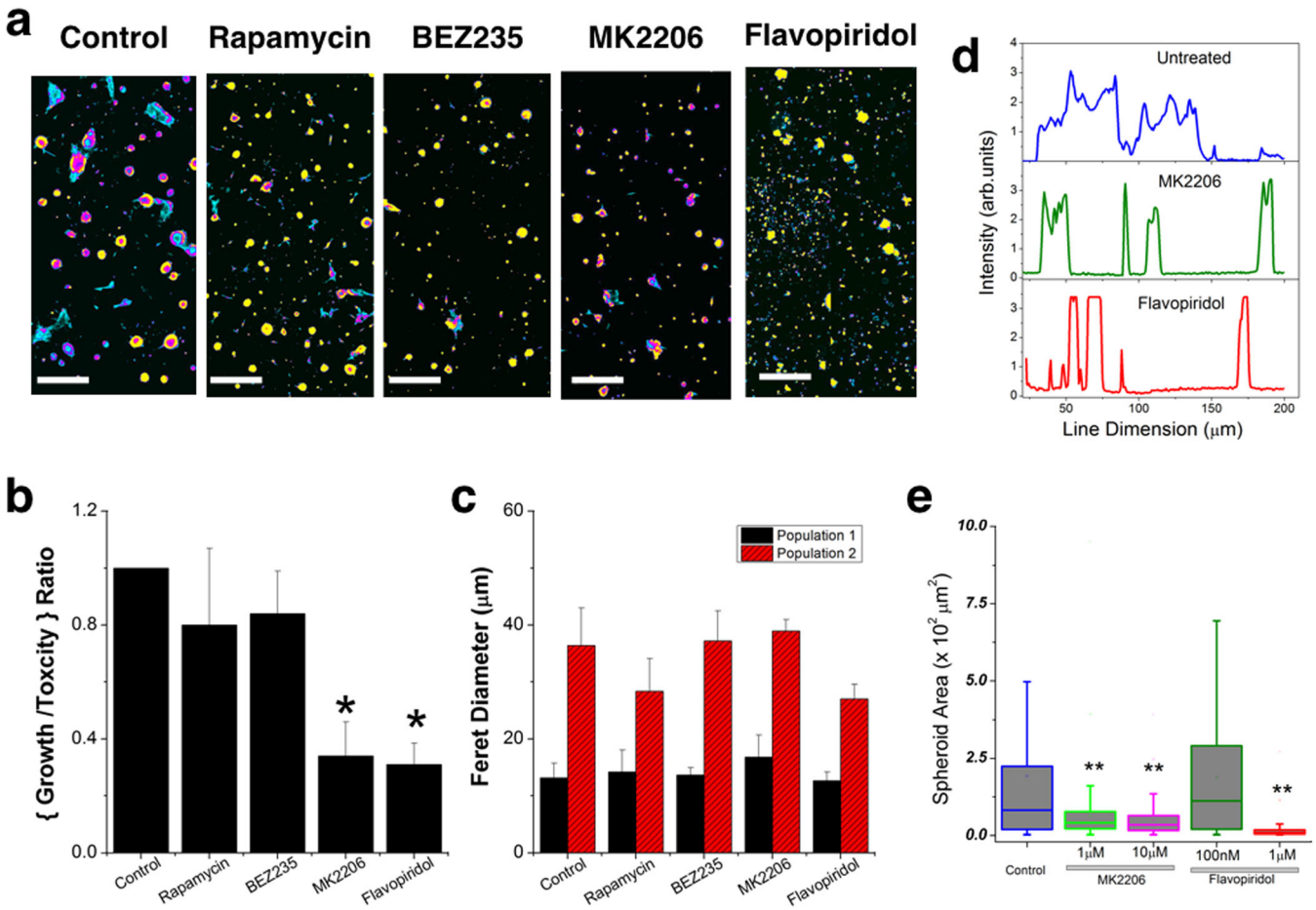

Fig. 4 Drug sensitivity assay in 3D tumor spheroids. **a** Representative images of 3D MMEpC spheroids were treated with drugs as indicated. Scale bars = 100 μm. Rapamycin is a mTOR inhibitor, BEZ235 is a dual ATP-competitive PI3K/mTOR inhibitor, MK2206 is a highly selective inhibitor of AKT 1/2/3, and flavopiridol is a cyclin-dependent kinase inhibitor. The concentrations used in this set of experiments were 500 nM rapamycin, 10 μM MK2206, 10 μM BEZ235, and 1 μM flavopiridol. **b** Seventy-two hours post-treatment, quantitative imaging analysis as described earlier was performed and the average {growth/toxicity} ratio from three independent trials is shown. Treatment with MK2206 and flavopiridol showed the most significant changes in {growth/toxicity} ratio. **c** Relative changes in the Feret diameters estimated from two-population Gaussian fit are shown for the untreated and drug-treated spheroids. **d** Representative line profiles show that the drug treatment significantly reduced the number and size of the larger spheroids as seen from the full width at half maximum (FWHM) of the peaks. **e** Concentration-dependent changes in spheroid size reveal that sub-optimal dosage of drug treatment (for, *e.g.*, 100 nM flavopiridol) can induce significant variance in the measurements.

vital factor associated with drug sensitivity and, hence, a potential biomarker. No significant difference was found between inter-spheroid heterogeneity measures (Suppl Fig. S4, see ESM). As a final demonstration of the utility of the approach developed here, we compared the drug sensitivity of six separate primary mammary tumor spheroids derived from six different sections of the same tumor isolated from PyMT inguinal mammary glands. As shown in Fig. 6a, these sections were spatially distinct—from the inguinal gland nipple region to the body cavity of the mouse. Figure 6b compares the averaged Feret diameter of the untreated and drug-treated spheroids, while Fig. 6c compares the {growth/toxicity} metric in each of these six groups of spheroids. Differential drug sensitivity in these six groups (intra-tumor heterogeneity) clearly supports the common wisdom that spatial heterogeneity in tumor response is more a norm than an aberration.

Discussion

Cellular heterogeneity manifests in a number of experimental measurements—from molecular traits (gene expression, protein interactions, *etc.*,) to physiological traits (*e.g.*, organ development) [5, 9, 24, 25]. Since tumors are inherently dynamic and are always adapting to rapidly changing microenvironment(s), one should expect a significantly higher extent of heterogeneity within the tumor mass, as demonstrated in this study. As mentioned in the

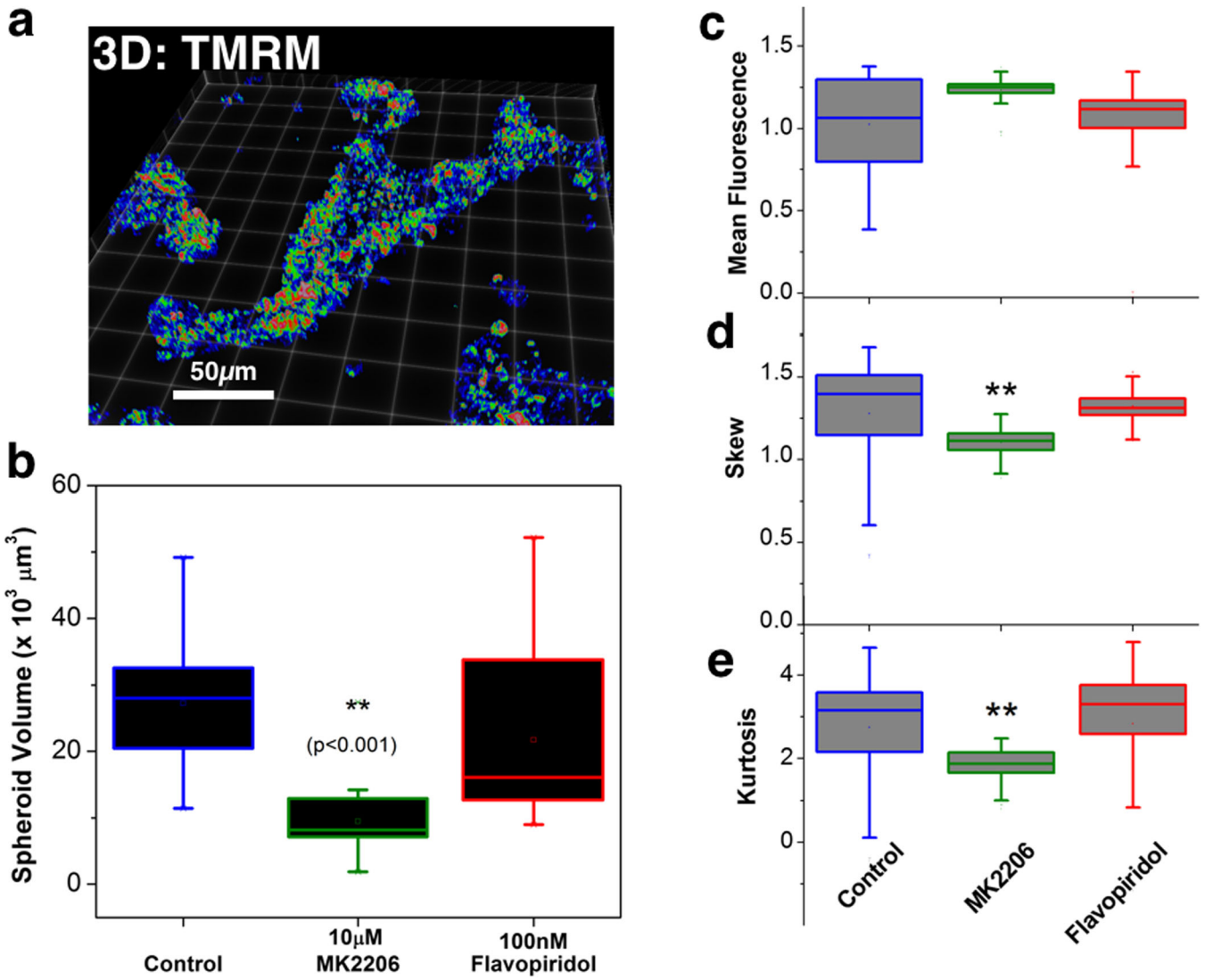

Fig. 5 Mitochondrial analysis in 3D spheroids adds value to the drug sensitivity determination. **a** 3D rendering of a typical spheroid labeled with mitochondrial membrane potential marker, TMRM shows spatial heterogeneity in mitochondrial activity. **b** 3D *xyz* confocal image stacks obtained from multiple spheroids were analyzed and the computed spheroid volumes are shown. Metabolic imaging results were in agreement with morphometric results as in Fig. 4. The *z* axis dependence of **c** mean TMRM fluorescence and its higher moments (**d** skew and **e** kurtosis) showed significant positive values for skew and kurtosis implying metabolic heterogeneity in the untreated spheroids. However, MK2206 treatment showed a significant reduction in this metabolic heterogeneity while 100-nM-flavopiridol treatment did not lead to any significant change in skew or kurtosis.

"Introduction" section, this study aimed to address three questions pertinent to quantitative characterization of 3D spheroids and their heterogeneous response to various drug treatments. The imaging work flow integrates morphometric and intensity measurements using ImageJ java script macros with custom-developed 3D *xyz* stack analyses using python codes. This basic framework also allows a variety of supervised and unsupervised classification (training and validation) approaches for predictive analytics using the same set of imaging data. As shown in Fig. 1f, there are multiple quantitative metrics that best describe the morphometric characteristics of tumor cells in 3D growth patterns. However, for the sake of simplicity, this study focused only on Feret diameter and its distribution. A fundamental parameter that is often measured in monolayer cell culture experiments is the cell viability which is less straightforward in 3D cultures. Commercially available kits (*e.g.*, Celltiter-Glo or MTT assay kits) require vigorous shaking and/or vigorous pipetting to extract the ATP and/or mitochondrial dehydrogenases, completely thereby inevitably disrupting the 3D spheroids. Owing to its luminescence readout, the Celltiter Glo assay could be more sensitive than the traditional MTT (absorbance) assay but the homogenization of the spheroids is a minimum requirement in both the assays. In contrast to these above methods, the imaging-based approach presented here uses morphometric measures

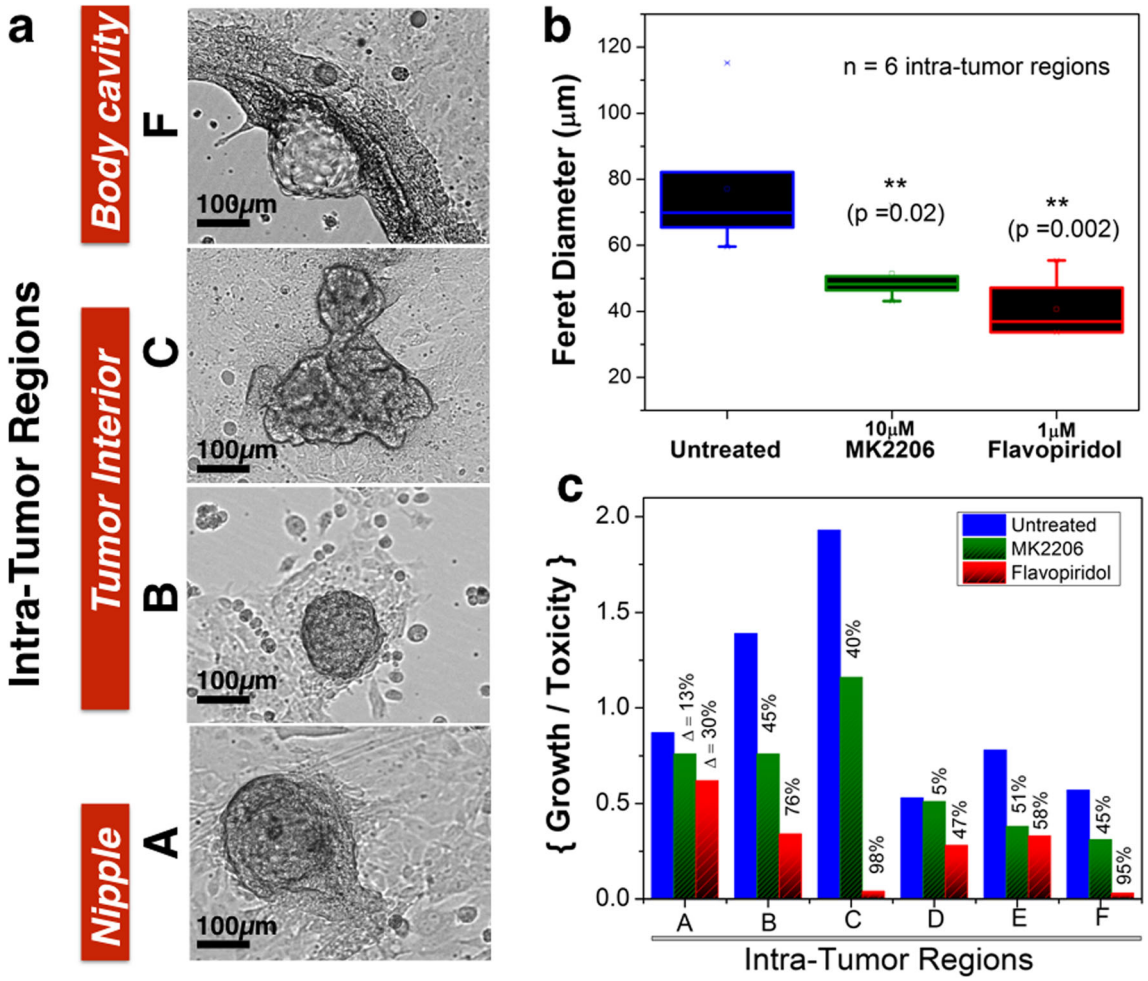

Fig. 6 Elucidating the degree of intra-tumor heterogeneity *via* 3D quantitative imaging. **a** Bright-field images of primary mammary spheroids derived from different sections of the same tumor as indicated. **b** 3D cultures of the primary mammary tumor epithelial cells from six intra-tumor regions were treated with either 10 μM MK2206 or 1 μM flavopiridol and image stacks analyzed as described earlier. All the six groups of 3D spheroids responded to the two drugs that were earlier shown to be efficacious. However, **c** these groups did exhibit significant heterogeneity in drug response as summarized in the {growth/toxicity} plots.

of spheroid growth with "minimally invasive" rupture of the spheroids to calculate growth/toxicity metric. The {growth/toxicity} ratio metric that is developed in this study has been demonstrated to be an excellent surrogate for cell viability in 3D mammary spheroids (see Suppl. Fig. S3, see ESM) Mitochondria have been earlier shown to be morphologically heterogeneous within individual cells, and since 3D spheroids have inherent oxygen gradients within them, it is expected that mitochondrial metabolism would exhibit spatial heterogeneity inside the spheroids [26–30]. It is interesting to note that higher moments of mean fluorescence, namely, the skew and the kurtosis parameters, can reliably track such metabolic heterogeneity within the spheroids (Fig. 3). Furthermore, since hypoxia-mediated drug resistance pathways have been linked to overall tumor resistance to chemotherapy and other targeted drugs, it is valuable to assess how such hypoxia and the associated mitochondrial metabolic heterogeneity within the spheroids can eventually determine the extent of drug sensitivity [31]. Regardless, the observation that 3D *xyz* stack analysis of mitochondrial metabolism within tumor spheroids is reflective of tracking hypoxic environment (Fig. 3) further adds value to the argument for monitoring mitochondrial metabolism in 3D architectures for a better understanding of drug sensitivity. In the author's laboratory, the effects of staining were tested on the cell metabolism, cell viability, and cell proliferation rates in a variety of cell lines and primary tumor cells. Based on these earlier tests, the protocol was optimized for using the lowest concentration of fluorogenic probes to yield a good signal-to-noise ratio in our imaging dataset. This optimization resulted in the final working concentration of the fluorophore staining as detailed in the "Materials and Methods" section. Furthermore, all live spheroid experiments were performed within ~90 min after

staining so that no compromise in cell viability or spheroid integrity due to staining was noticed. Traditionally, mean fluorescence is a key parameter that is monitored in any imaging dataset. However, an extensive analysis of the dataset in this study led to the discovery that the higher moments of the fluorescence intensity, *i.e.*, skew and kurtosis, shed more light on the spatial heterogeneity of mitochondrial metabolism (Fig. 3). Since these parameters showed distinct *z*-profile only in TMRM fluorescence (a functional mitochondrial probe) and not in mitotracker green fluorescence (a vital stain that does not indicate the functional differences in mitochondria), these results point out to an interesting possibility that the skew and the kurtosis parameters can potentially complement the traditional cell viability and growth/toxicity measures used in the drug screening. More experiments and systematic validation may be required to establish the link between drug response and the "heterogeneity indices" identified in this study. The observation that the inter-spheroid heterogeneity did not change significantly (Suppl. Fig. S4, see ESM) might have stemmed from the fact that these spheroids do not have microenvironment akin to the tumors *in vivo*. In addition to the murine 3D spheroids presented here, the proposed method was successfully tested in 3D spheroids generated from two other human breast cancer cell lines (MDA-MB-231 and BT-549) (Suppl Fig. S5, see ESM), further confirming the general applicability of the image analysis procedures discussed here. This author would like to iterate that this study is the first step in the general direction of developing an integrated image analysis platform in realistic, tumor specimens with multiple components (vasculature, immune cells, fibroblasts, *etc.*,) along with the breast cancer spheroids. From the physiological standpoint, the current study is more relevant to avascular tumor nodules and distant metastatic tumor niche and the lymph node metastatic nodules. Co-culture experiments with tumor epithelial cells and immune factors and stromal fibroblasts as well as including angiogenic components might shed more light on the roles of inter-spheroid heterogeneity in drug response traits.

Finally, the findings of this study concur with the current wisdom that not all the regions within a tumor mass exhibit uniform drug sensitivity and the fact that 3D mammary spheroids derived from spatially distinct tumor regions exhibit varying drug sensitivity—points out to an interesting possibility that the image analysis framework presented here, can be a valuable tool box in high-throughput 3D drug screening assays. At this point, there is not enough data to determine if there is any fundamental relationship between drug response and the spatial location of the tumor (as seen in Fig. 6). This author believes that the observed differential response might arise from a number of factors such as the nutrient availability, relative proportion of proliferative *vs* non-proliferative cells within the tumors.

Conclusions

In conclusion, the integrated, quantitative imaging protocols described in this paper can find utility in characterizing 3D tumor spheroids—beyond the examples presented here. The physiological relevance of this study is that the analyses described here can be used to understand the avascular tumor spheroids—that were recently demonstrated to be the early precursors of tumor growth *in vivo* as well as lymph node metastatic nodules [32, 33]. It is envisioned that with further developments in real-time analysis modules, the current approach can be used for characterizing 3D tumor nodules in biopsies *ex vivo*, as well as in intact tumors in human patients.

Acknowledgements. The author gratefully acknowledges Bruce Gewertz, MD, for his continuous support and inspiration.

Funding Information. Financial support was provided by American Cancer Society (RSG-12-144-01-CCE), National Cancer Institute/National Institutes of Health (R21-CA124843), Komen for the Cure Foundation (KG090239), and Donna & Jesse Garber Foundation.

Compliance with Ethical Standards

Conflict of Interest

The author declares that he has no conflict of interest.

References

1. Hanahan D, Weinberg RA (2011) Hallmarks of cancer: the next generation. Cell 144:646–674
2. Tennant DA, Duran RV, Boulahbel H, Gottlieb E (2009) Metabolic transformation in cancer. Carcinogenesis 30:1269–1280
3. Narod S (2016) Breast cancer: the importance of overdiagnosis in breast-cancer screening. Nat Rev Clin Oncol 13:5–6
4. Martelotto LG, Ng CK, Piscuoglio S et al (2014) Breast cancer intra-tumor heterogeneity. Breast Cancer Res 16:210
5. Potts SJ, Krueger JS, Landis ND, Eberhard DA, David Young G, Schmechel SC, Lange H (2012) Evaluating tumor heterogeneity in immunohistochemistry-stained breast cancer tissue. Lab Investig 92:1342–1357
6. Sengupta D, Pratx G (2016) Imaging metabolic heterogeneity in cancer. Mol Cancer 15:4
7. Kim JB, O'Hare MJ, Stein R (2004) Models of breast cancer: is merging human and animal models the future? Breast Cancer Res 6:22–30
8. Hu Z, Fan C, Oh DS, Marron JS, He X, Qaqish BF, Livasy C, Carey LA, Reynolds E, Dressler L, Nobel A, Parker J, Ewend MG, Sawyer LR, Wu J, Liu Y, Nanda R, Tretiakova M, Orrico A, Dreher D, Palazzo JP, Perreard L, Nelson E, Mone M, Hansen H, Mullins M, Quackenbush JF, Ellis MJ, Olopade OI, Bernard PS, Perou CM (2006) The molecular portraits of breast tumors are conserved across microarray platforms. BMC Genomics 7:96
9. Elsasser WM (1984) Outline of a theory of cellular heterogeneity. Proc Natl Acad Sci U S A 81:5126–5129
10. Ma Z, Shiao SL, Yoshida EJ, Swartwood S, Huang F, Doche ME, Chung AP, Knudsen BS, Gertych A (2017) Data integration from pathology slides for quantitative imaging of multiple cell types within the tumor immune cell infiltrate. Diagn Pathol 12:69
11. Simian M, Bissell MJ (2017) Organoids: a historical perspective of thinking in three dimensions. J Cell Biol 216:31–40

12. Friedrich J, Seidel C, Ebner R, Kunz-Schughart LA (2009) Spheroid-based drug screen: considerations and practical approach. Nat Protoc 4:309–324
13. Lin EY, Jones JG, Li P, Zhu L, Whitney KD, Muller WJ, Pollard JW (2003) Progression to malignancy in the polyoma middle T oncoprotein mouse breast cancer model provides a reliable model for human diseases. Am J Pathol 163:2113–2126
14. Ramanujan VK (2019) Rapid assessment of mitochondrial complex I activity and metabolic phenotyping of breast cancer cells by NAD(p)H cytometry. Cytometry Part A 95:101–109
15. Ramanujan VK (2014) Metabolic imaging in multiple time scales. Methods 66:222–229
16. Najafi M, Soltanian-Zadeh H, Jafari-Khouzani K, Scarpace L, Mikkelsen T (2012) Prediction of Glioblastoma Multiform Response to Bevacizumab Treatment Using Multi-Parametric MRI. PLoS One 7:e29945
17. Stottrup C, Tsang T, Chin YR (2016) Upregulation of AKT3 confers resistance to the AKT inhibitor MK2206 in breast Cancer. Mol Cancer Ther 15:1964–1974
18. Wang H, Huang F, Wang J, Wang P, Lv W, Hong L, Li S, Zhou J (2015) The synergistic inhibition of breast cancer proliferation by combined treatment with 4EGI-1 and MK2206. Cell Cycle 14:232–242
19. Tan AR, Swain SM (2002) Review of flavopiridol, a cyclin-dependent kinase inhibitor, as breast cancer therapy. Semin Oncol 29:77–85
20. Tong CWS, Wu M, Cho WCS, To KKW (2018) Recent advances in the treatment of breast Cancer. Front Oncol 8:227
21. Kalinsky K, Sparano JA, Zhong X, Andreopoulou E, Taback B, Wiechmann L, Feldman SM, Ananthakrishnan P, Ahmad A, Cremers S, Sireci AN, Cross JR, Marks DK, Mundi P, Connolly E, Crew KD, Maurer MA, Hibshoosh H, Lee S, Hershman DL (2018) Pre-surgical trial of the AKT inhibitor MK-2206 in patients with operable invasive breast cancer: a New York Cancer consortium trial. In: Clin Transl Oncol, vol 20, pp 1474–1483
22. Blagosklonny MV (2004) Flavopiridol, an inhibitor of transcription: implications, problems and solutions. Cell Cycle 3:1537–1542
23. Mukherjee B, Tomimatsu N, Amancherla K, Camacho CV, Pichamoorthy N, Burma S (2012) The dual PI3K/mTOR inhibitor NVP-BEZ235 is a potent inhibitor of ATM- and DNA-PKCs-mediated DNA damage responses. Neoplasia 14:34–43
24. Trilla-Fuertes L, Gamez-Pozo A, Arevalillo JM et al (2018) Molecular characterization of breast cancer cell response to metabolic drugs. Oncotarget 9:9645–9660
25. Xu HN, Zheng G, Tchou J, Nioka S, Li LZ (2013) Characterizing the metabolic heterogeneity in human breast cancer xenografts by 3D high resolution fluorescence imaging. Springerplus 2:73
26. Bellance N, Lestienne P, Rossignol R (2009) Mitochondria: from bioenergetics to the metabolic regulation of carcinogenesis. Front Biosci 14:4015–4034
27. Kroemer G (2006) Mitochondria in cancer. Oncogene 25:4630–4632
28. Collins TJ, Bootman MD (2003) Mitochondria are morphologically heterogeneous within cells. J Exp Biol 206:1993–2000
29. Ye XQ, Wang GH, Huang GJ, Bian XW, Qian GS, Yu SC (2011) Heterogeneity of mitochondrial membrane potential: a novel tool to isolate and identify cancer stem cells from a tumor mass? Stem Cell Rev 7:153–160
30. Kuznetsov AV, Margreiter R (2009) Heterogeneity of mitochondria and mitochondrial function within cells as another level of mitochondrial complexity. Int J Mol Sci 10:1911–1929
31. Rohwer N, Cramer T (2011) Hypoxia-mediated drug resistance: novel insights on the functional interaction of HIFs and cell death pathways. Drug Resist Updat 14:191–201
32. Orme ME, Chaplain MA (1996) A mathematical model of the first steps of tumour-related angiogenesis: capillary sprout formation and secondary branching. IMA J Math Appl Med Biol 13:73–98
33. Chaplain MA, Anderson AR (1996) Mathematical modelling, simulation and prediction of tumour-induced angiogenesis. Invasion Metastasis 16:222–234